Journal of Advanced Research 66 (2024) 237–249

Contents lists available at ScienceDirect

Journal of Advanced Research

journal homepage: www.elsevier.com/locate/jare

Original Manuscript

Hierarchical double-layer microneedles accomplish multicenter skin regeneration in diabetic full-thickness wounds

Xiaoqi Huang [1], Xingtang Niu [1], Yuan Ma [1], Xinhui Wang, Ting Su, Yu He, Feng Lu *, Jianhua Gao *, Qiang Chang *

Department of Plastic and Cosmetic Surgery, Nanfang Hospital, Southern Medical University, 1838 Guangzhou North Road, Guangzhou 510515, Guangdong, China

HIGHLIGHTS

- A novel multicentric regeneration model capable of fusing to form a complete full-thickness skin.
- Bilayer microneedles are utilized to combine the synergistic action of epidermal and dermal cells.
- A layered scaffold that conforms to the skin structure, achieving functional skin regeneration.
- The density of MNs was verified to ensure optimal cellular cross-talk between different cells.
- The microneedle tip accurately delivers cells to the corresponding area.

GRAPHICAL ABSTRACT

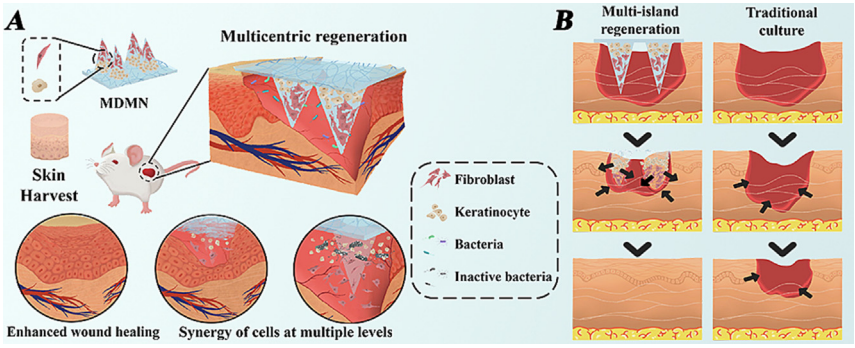

ARTICLE INFO

Article history:
Received 4 May 2023
Revised 12 December 2023
Accepted 3 January 2024
Available online 11 January 2024

Keywords:
Antibacterial
Chronic
Diabetic
Microneedle
Omnidirectional

ABSTRACT

Introduction: Managing large chronic wounds presents significant challenges because of inadequate donor sites, infection, and lack of structural support from dermal substitutes. Hydrogels are extensively used in various forms to promote chronic wound healing and provide a three-dimensional spatial structure, through growth factors or cell transport.

Objectives: We present a novel multicenter regenerative model that is capable of regenerating and merging simultaneously to form a complete layer of skin. This method significantly reduces wound healing time compared to the traditional centripetal healing model. We believe that our model can improve clinical outcomes and pave the way for further research into regenerative medicine.

Methods: We prepared a novel multi-island double-layer microneedle (MDMN) using gelatin-methacryloylchitosan (GelMA-CS). The MDMN was loaded with keratinocytes (KCs) and dermal fibroblasts (FBs). Our aim in this study was to explore the therapeutic potential of MDMN in a total skin excision model.

Results: The MDMN model replicated the layered structure of full-thickness skin and facilitated tissue regeneration and healing via dual omni-bearing. Multi-island regeneration centres accomplished horizontal multicentric regeneration, while epidermal and dermal cells migrated synchronously from each location. This produced a healing area approximately 4.7 times greater than that of the conventional scratch tests. The MDMN model exhibited excellent antibacterial properties, attributed to the chitosan layer. During wound healing in diabetic mice, the MDMN achieved earlier epidermal coverage and faster wound healing through multi-island regeneration centres and the omnidirectional regeneration mode. The MDMN group displayed an accelerated wound healing rate upon arrival at the destination

* Corresponding authors.
E-mail address: doctorchq@smu.edu.cn (Q. Chang).
[1] These authors contributed equally.

https://doi.org/10.1016/j.jare.2024.01.002
2090-1232/

(0.96 % ± 0.58 % vs. 4.61 % ± 0.32 %). Additionally, the MDMN group exhibited superior vascularization and orderly collagen deposition.
Conclusion: The present study presents a novel skin regeneration model using microneedles as carriers of autologous keratinocytes and dermal fibroblasts, which allows for omni-directional, multi-center, and full-thickness skin regeneration.

Introduction

An ongoing concern in clinical practice is the management of chronic wounds, particularly those caused by diabetes and ulcers [1–3]. Delayed wound heightens increases the risk of nfections and significantly aggravates skin barrier function and overall quality of life [4,5]. The present clinical approach to managing chronic wounds comprises procedures such as skin flap grafting [6], debridement, and traditional dressings (e.g., gauze and bandages) [7–9], as well as bioengineered skin [10,11]. While these methods have their constraints, including a shortfall of donor sites for flap transplantation, multiple skin transplants, and the infusion of growth factors, they retain the potential for further enhancement [12–15].

Meek's skin micrografting technique and skin substitute products provide a viable solution to the problem of limited donor sites [16]. A stratified skin (STS), comprising the epidermis and part of the dermis, was obtained from the donor site and then diced into skin particles of 0.3–0.8 mm^2 for transplantation [17]. The Meek skin micrografting technique has a remarkable skin graft expansion rate with an expansion ratio of up to 1:4–1:9, thereby reducing the need for donor site skin and allowing for excellent re-epithelialization rates. Furthermore, patients treated with the Meek method manifest a lower graft failure rate than those undergoing whole flap transplantation because of micrografts that act as autonomous regenerative centers [18–21]. It should be noted that these micrografts do not contain dermal elements and mainly depend on re-epithelialization for wound healing, which can lead to scar formation and wound contracture. Additionally, the skin substitute creates a microenvironment similar to that of the extracellular matrix, thereby reducing the healing time for wounds and enhancing the skin's barrier function [22,23]. However, fully homogenised skin substitutes are not entirely suitable for the natural structure of the skin, posing a challenge to complete skin regeneration [24].

During the process of wound healing, various cellular and extracellular pathways are activated in a meticulously regulated and coordinated manner to restore the integrity of tissues [25]. Epidermal cells, in particular, play a crucial role in wound healing through re-epithelialisation, which is a vital marker of wound closure [25]. Similarly, fibroblasts, by secreting collagen and forming granulation tissue, are crucial in maintaining the strength and integrity of tissues during the wound healing process [26]. However, numerous other cell types, comprising immune cells like neutrophils, macrophages, and lymphocytes, are also engaged in the wound healing process and have significant roles in clearing debris and remodelling tissue. The emergence of blood vessels during angiogenesis is a crucial aspect of granulation tissue, as they deliver oxygen, nutrients, and bioactive substances to the wound area, highlighting their essential role in wound healing. Furthermore, endothelial cells facilitate the chemotaxis of inflammatory cells from blood vessels to damaged skin tissues. These inflammatory cells then release inflammatory factors and extracellular matrix, which encourage the proliferation of basal cells.

Delivering these two types of cells in the correct temporal and spatial order in the wound has the potential to build natural skin layers. Microneedles (MNs) are an excellent candidate for simulating and engineering full-thickness skin structures. These miniature needles offer an array of advantages, with their needle tip serving as a self-regeneration center that can facilitate multi-layered collagen production in a longitudinal direction. This collaborative approach ensures a more accurate simulation of the natural skin structure, ultimately leading to improved cosmetic outcomes. Compared with traditional dressings, MNs have micron-scale needle tips, allowing for effectively delivering coated cells or bioactive substances to the corresponding tissue areas [27]. MNs have demonstrated their value in multiple disease treatments, including wound healing [28], vaccine delivery [29], and in situ detection [30]. Importantly, owing to the lack of connectivity between the tips, the inactivation of cells encapsulated within a single tip does not adversely affect cells at other tips. GelMA, a photo-crosslinked polymer derived from gelatin, is a widely used biomaterial for MN applications due to its good biocompatibility and cell responsiveness [31–33]. After photocrosslinking, GelMA can sustainably release encapsulated small molecules and cells [34,35], making it a versatile biomaterial for various biological applications and tissue engineering [36–39]. In addition, chronic wound healing has been linked to an increased risk of infection, prolonged infection, and even life-threatening infection. To mitigate this risk and safeguard the cells from contamination during the healing process, we incorporated chitosan (CS) into our approach. CS, a positively charged linear amino polysaccharide composed of approximately 80 % β1,4-linked D-glucosamine (GlcN) and 20 % β1,4-linked N-acetyl-D-glucosamine (glucosamine), is derived from crustaceans or fungal shells. This substance has garnered widespread applications in biomedicine and tissue engineering scaffolds due to its biocompatibility, low toxicity, biodegradability, and antibacterial effect [40–43]. By leveraging the wound-healing capabilities of CS, we aim to reduce the risk of infection and promote cell survival during the healing process.

In this study, we have successfully constructed a multi-island double-layered microneedle (MDMN) using GelMA hydrogel infused with KCs and FBs, which mimics the natural skin structure and multi-island regenerative centers of MEEK micrografting technology. This innovative approach provides an effective tool for dermatological regenerative medicine. Fig. 1 illustrates the process of creating a GelMA prepolymer by mixing KCs and FBs obtained from autologous full-thickness skin with a GelMA solution. The prepolymer was then poured into a polydimethylsiloxane (PDMS) mold, following the sequential pattern of the skin layers, with GelMA-CS integrated as the backing material. After vacuum defoaming and UVA cross-linking, we obtained MDMNS structures that mimic skin. The vertical layers of microneedles followed the same hierarchical ratio as normal skin, which was demonstrated by adjusting the needle density. This adjustment also had an impact on the directional migration of cells. The tip of the needle serves as the regeneration centre of the micro-skin island, and the density of its distribution holded paramount importance in regulating cell biological behaviour and wound healing. In the case of diabetic and normal wounds, animals treated with MDMN showed an improved healing rate, increased re-epithelialization, promoted angiogenesis, and increased expression of related proteins. These results demonstrate that longitudinally stacked double-layered

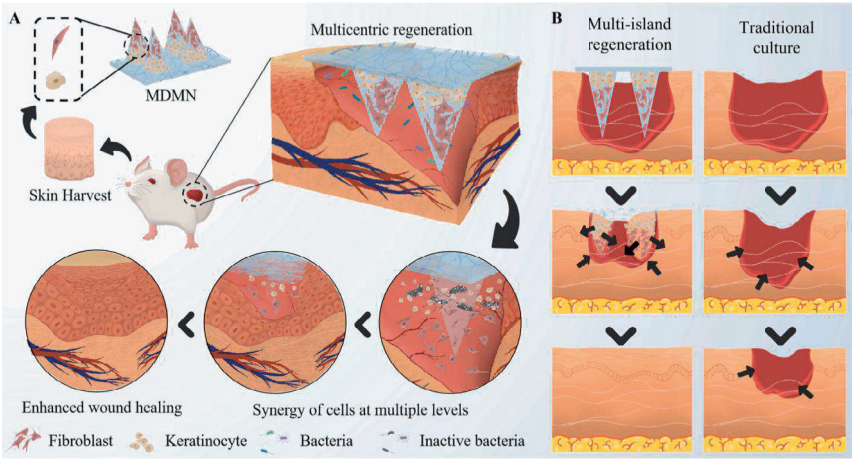

Fig. 1. (A) The design and application of the MN system loaded with KCs, FBs, and chitosan. (B) Multi-island regeneration compared with traditional culture, the arrow shows the direction of regeneration.

MDMNs achieve omnidirectional multi-centric regeneration by delivering KCs and FBs as well as synergistically promoting cell migration, representing a completely new mode of regenerative healing.

Materials and methods

Materials and cell cultures

Methacrylic anhydride (purity = 94 %), gelatin (type A, gel strength 200, from pigskin), and the photoinitiator 2-hydroxy-(4-(hydroxyethyl)benzene base)-2-methyl-1-propanone(Irgacure 2959) were purchased from Macklin (Shanghai, China). Chitosan (low viscosity, <200 mPa.s) and calcein were purchased from Aladdin (Shanghai, China). The cells used in this experiment, including FBs and KCs, were obtained from the full-thickness skin of C57BL/6J mice. For the study of normal wounds, FBs and KCs were extracted from the skin tissues of non-diabetic mice, whereas diabetic wound models used FB and KC obtained from STZ-induced T2D mice. After harvesting, the cells were cultured in high-glucose DMEM (Gibco) supplemented with 10 % fetal bovine serum (FBS; Gibco) and 1 % penicillin–streptomycin (Gibco). Tissue passage or harvesting was done after 80 % fusion was reached. Third to sixth generation FBs and KCs were used in this experiment.

Preparation of GelMA

GelMA was prepared using a method previously reported [31]. Briefly, a 10 % w/v gelatin was dissolved in PBS (pH 4.7) at around 50 °C with constant stirring. Then, a specific amount of methacrylic anhydride was introduced under vigorous magnetic stirring. The resulting mixture was continuously stirred at 50 °C for a duration on 120 min. Finally, 5 × PBS was added to halt the methacrylate modification. Following this, the mixture underwent dialysis in distilled water for a week utilizing a 12–14 kDa dialysis membrane. The functionalized gelatin was subsequently frozen and lyophilized, then stored at −80 °C to allow for further utilization. GelMA underwent characterization through Fourier transform infrared (FTIR) spectroscopy (Mattson Instruments Inc., model Genesis II, Madison, WI, USA).

Preparation of MDMN

The MDMN was produced in a biologically secure cupboard under strict hygienic conditions. First, 5 g of GelMA was dissolved in 50 mL of PBS solution at 37 °C. Then, 25 mg of photoinitiator (Irgacure 2959) was introduced to the solution. Three mixed solutions of FB-GelMA (10^6/mL), KC-GelMA (10^6/mL), and CS-GelMA (3 % w/v) were prepared by dividing the GelMA solution into three parts and adding FBs, KCs, and CS, respectively. The PDMS mold was filled with 300uL of FB-GelMA and placed under vacuum at 37 °C for 5 min to remove any surface air bubbles.A small quantity of FB-GelMA was then removed from inside the tip, after which 100uL of KC-GelMA was added to evacuate the vacuum for 2 min until the tip was filled. Next, CS-GelMA was added to fill the bottom groove as a backing. Finally, the molds were placed under to 10 mW/cm^2 of UV light (365 nm) for 3 min to crosslink. After the crosslinking was completed the MDMN was carefully peeled off the PDMS mold and used immediately. The molds were prismatic conical tips with a tip height of 850 μm, a tip base diameter of 410 μm, a backing groove depth of 10 mm, and tip spacings of 2000 μm (MN I), 1500 μm (MN II), 1000 μm (MN III), and 500 μm (MN IV), respectively, and a total of four PDMS molds were used to fabricate the MDMN.

Scanning electron microscopy

To assess the physical morphology of the MDMN patches, all samples were analyzed using a scanning electron microscope (FEI, Nova NanoSEM 450, USA) operated at an accelerating voltage of 5 kV. The samples were spray-coated with gold to increase conductivity before imaging.

Biocompatibility of the GelMA hydrogel and MDMNs in vitro

FBs and KCs were cultured at a seeding density of 1 × 10^5 per well on a 6-well plate covered with GelMA hydrogel at the bottom and incubated at 37 °C for 24 h. Live/dead detection kits were used for fluorescence staining. On days 1, 3, and 5, use calcein AM (1 μL/mL of 50 μM stock, green, 494/517 nm) and ethidium homodimer-1 (2 μL/mL of 2 mM stock solution, red, 528/617 nm) were used, and fluorescence images were collected at 10 × magnification using an inverted fluorescence microscope (Olympus IX 73). The total number of live and dead cells was quantified using the ImageJ software. Cell proliferation was quantified by calculating the average number of viable cells with positive staining per frame.

Biocompatibility of the MDMN patches was assessed by KCs and FBs viability. Briefly, sterile MDMN patches were immersed in Transwell chambers containing 1 % FBS high-glucose complete medium (3 mL/well) for 3 days, and then the chambers were

removed to obtain extracts of the MN patches. Next, FBs and KCs were then inoculated into a 96-well plate (1×10^3/well), and 100 uL of the extract was added to each well. The cytotoxicity of the sterile microneedle extracts to FBs and KC swas determined using the CCK8 assay on days 1, 3, and 5.

Wound healing by scratch assay in vitro

L929 mouse fibroblasts were seeded in 6-well plates (1×10^5/well) and incubated for 24 h. The next day, they were scratched with a 200-uL pipette tip. They were then placed in transwell chambers containing different groups of microneedles (native MN, KC MN, FB MN, and MDNM), and scratch healing was recorded at 0, 24, 48, and 72 h. Images were analyzed using Image J. Wound healing rate = (original wound area − current measured area)/original wound area × 100 %.

Quantification of cytokine secretion in vitro

Different microneedle groups (native MN, KC MN, FB MN, and MDNM) were cultured in serum-free media for 24 h. After the incubation period, the supernatant fluid was collected. The levels of LPS, KGF, TNF-α, TGF-α, IL-1α, IL-1β, FGF, EGF, and TGF-β were quantified using ELISA kits following the manufacturer's instructions (Jiangsu Meimian Industrial Co., Ltd.). Briefly, 50 μL of the collected supernatant was aspirated and applied to the wells of a 96-well inline plate pre-coated with the capture antibody. The plate was then incubated for 30 min at 37 °C and washed thoroughly. Subsequently, 50 μL of biotinylated detection antibody was added to each well, followed by an additional 30-minute incubation at 37 °C. After extensive washing, 3,3′,5,5′-tetramethylbenzidine substrate solution was added, and the plates were incubated in the dark for 10 min at room temperature. Finally, 50 μL of termination solution was added to each well, and the absorbance at 450 nm was recorded using a microplate reader.

Antibacterial test in vitro

The bactericidal activity of the samples was tested against *Staphylococcus aureus* (ATCC 29213) and *Escherichia coli* (ATCC 25922). After transferring sterile MNs were transferred to a 48-well plate, 100 μL of the bacterial solution was added, and the mixture was incubated for 4 h at 37 °C. Then add 900 μL of medium was added and incubated overnight in a CO_2 incubator. After 24 h of incubation, the absorbance was measured at 600 nm using a microtiter plate reader. A bacterial solution to which no sample was added was used as a control. Finally, the bacterial culture was diluted to the appropriate concentration (10^3 CFU/mL). Bacterial colonies were counted after 6 h, 12 h and 24 h.

Animal wound healing experiments

The T2D mouse model was established by injecting STZ (100 mg/kg) into 6-week-old male C57BL/6J mice after 2 weeks of high-fat chow feeding [44]. Blood samples were taken from the tail vein of the mice prior to the experiment. Blood glucose levels were then measured utilizing a blood glucose meter (Sinocare Inc., Changsha, China). After the blood glucose level reached a stable hyperglycaemic state, a full-thickness skin defect model with a diameter of 10 mm was created on the dorsal skin of 6-week-old male C57BL/6J mice. The mice were randomly divided into five groups (n = 3 mice per group): control, native MN, KC MN, FB MN, and MDMN. On days 8 and 18 after treatment, the animals were killed and their wound sites photographed. In addition, simple wounds were used to compare the therapeutic efficacy of MDMN with a commercially available recombinant growth factor gel (Pavay Inc., Guilin, China). A 10 mm adiameter full-thickness skin defect mod was established on the dorsal skin of 8-week-old male C57BL/6J mice. Mice were randomly divided into 6 groups (n = 3 mice per group): control, native MN, KC MN, FB MN, MDMN, and growth factor gel (GF) [45–48]. Animals were killed and the wound site was photographed on days 7 and 14 after treatment.

Histopathology assay

After 14 and 18 days of treatment, each mouse was sacrificed, and the wound samples from each group were randomly selected for histological examination, with normal skin as the control. The skin tissues were fixed in 4 % buffered paraformaldehyde overnight and then embedded in paraffin. The samples were sectioned and stained with hematoxylin-eosin (H&E) and Masson's trichrome. The epidermal thickness was evaluated by examining the H&E-stained specimens. Collagen synthesis was demonstrated through Masson's trichrome staining. The sections were rehydrated and citric acid buffer and heat were sued for antigen retrieval. Subsequently, they were permeabilized with 1 % Triton X-100 solution for 30 min and blocked for 2 h in a solution of 2 % BSA and 2 % goat serum. Antibodies against PCNA (Abcam) and CD31 (Abcam) were diluted at a 1:100 and incubated with sections overnight at 4 °C. After being washed in tris-buffered saline solution containing 0.01 % tween-20 (TBS-T, pH 7.4), the sections were incubated with HRP-conjugated goat anti-rabbit IgG for 2 h, reacted with diaminobenzidine, counterstained with hematoxylin or incubated with Alexa-Fluor conjugated secondary antibodies (Invitrogen) for 2 h, washed with TBS-T, counterstained with DAPI, and covered using a coverslip.

Ethics statement

Animal experiments were conducted in accordance with the guidelines of the National Health and Medical Research Committee (People's Republic of China) and approved by the Ethics Committee of Nanfang Hospital (NFEC-2019-212). We obtained ethical approval for all experimental procedures to ensure the humane treatment of the animals (IACUC-LAC-20221125-003). Additionally, all applicable institutional and national guidelines for the care and use of animals were adhered to.

Statistical analysis

All data were presented as the mean ± standard deviation (SD). Each experiment was conducted a minimum of three times. Statistical significance was determined using two-way ANOVA with Tukey's post-hoc test. GraphPad Prism version 9.4 was used for all statistical analyses. 'ns' signifies non-significance unless otherwise indicated. '* $p < 0.05$', '** $p < 0.01$', and '*** $p < 0.001$' denote statistical significance.

Results and discussions

Preparation and characterization of MDMN

GelMA was synthesised by modifying gelatin with methacrylic anhydride. The success of this modification was confirmed by the Fourier transform infrared spectroscopy (FTIR) spectra, which were obtained for both gelatin and GelMA (Fig. S1). The absorption bands at 3308 and 3079 cm^{-1} were attributed to the N–H stretching of the amide A band and the C–H stretching of the amide B band, respectively. Furthermore, the peaks at 1645, 1549, and 1241 cm^{-1} were attributed to the C═O stretching of the amide I bond, N–H bending and C–N stretching of the amide II band, and N–H bending of the

amide III band, respectively. The wavenumber of the amide II band and the presence of the amide III band confirmed the secondary amide structure in GelMA. These results confirm the successful fabrication of GelMA. The fabrication process for the MDMN is shown in Fig. 2A. The patches were prepared using the micromolding method, in which three GelMA prepolymers were vacuum cast in a layered fashion into pre-designed molds. The prepared MNs exhibited an 11 × 11 uniformly arranged array (Fig. 2B). In the scanning electron microscope (SEM) image, the MN is cone-shaped, with a height of approximately 800 μm and a base diameter of approximately 400 μm (Fig. 2C and D). The unique morphology of the MNs significantly increases their specific surface area, thus facilitating the release of bioactive factor and providing sufficient contact with the surrounding tissue. The needle tip was layered according to the normal mouse skin structure (Fig. 2E (i)). The red fluorescent cell membrane probe DiI and the green fluorescent cell membrane probe DiO were used to label the KCs and FBs in the MN, and the KCs and FBs were observed in different layers of the microneedles. Frozen sections (Fig. 2E (ii)) and confocal microscopy (Fig. 2E (iii)) clearly show the hierarchical structure of the double-layered microneedles in proportion to that of the epidermis and dermis.

MDMN biocompatibility and needle spacing

Biocompatibility is a critical factor in assessing the quality of biomaterials. To test cell viability and proliferation, a live/dead cell staining assay was conducted, and the results indicated that the GelMA hydrogel exhibited excellent cell viability (Fig. 3A). The cytotoxicity of the hydrogel microneedles was evaluated using the CCK-8 assay. As shown in Fig. 4C, after 5 days of incubation, cell viability continued to increase in all hydrogel groups, consistent with the control group, reflecting the ideal cytocompatibility of the hydrogels. The MDMN group was stimulated by bi-cellular secretion of active factors and showed higher cell viability compared to the control group. We then used ELISA to measure different groups of lipopolysaccharide (LPS) to further verify its safety. There was no significant difference in LPS between all microneedle groups (Native MN: 4.17 ± 2.42 vs KC: 5.26 ± 0.23 vs FB: 4.40 ± 0.11 vs MDMN: 4.67 ± 0.57 ng/L) and was far below the safety standard line, indicating that they all have good biosafety [49].

The needle tip is the regeneration centre of the micro-skin island, and the distribution density of the regeneration centre is of great importance in regulating of cell biological behaviour and wound healing. Increasing the needle density multiplies the specific surface area of the MN and enhances the resistance to deformation caused by the directional cell migration and growth. This process favours tissue regeneration. However, excessive needle density results in increased hydrophobicity, which has the potential to limit cell migration and proliferation [50].

To investigate the interaction between needle spacing and tissue, four needle spacings of 2000, 1500, 1000, and 500 μm were defined as MN I, MN II, MN III, and MN IV (Fig. S2), respectively. First, the effects of a single tip on cell growth and proliferation were assessed. Confocal microscopy images showed that the number of cells within the tip of the four groups increased significantly after five days (Fig. 3B), and there was no statistically significant difference in proliferation among MN I (10.92 % ± 0.11 %), MN II (10.21 % ± 0.20 %), MN III (10.42 % ± 0.92 %), and MN IV (10.65 % ± 1.12 %) (Fig. 3D). The results showed that changes in the needle density had no significant effect on cell proliferation within the needle tip. Next, the effect of needle density on directional migration of cells was evaluated. Compared with the MN I group (3.30 % ± 0.32 %), the MN II (3.71 % ± 0.03 %), MN IV (4.69 % ± 0.26 %), and MN III groups (5.45 % ± 0.30 %) had higher mobility (Fig. 3C, E and S3). These results suggest that increasing needle density has a positive effect on targeted cell migration. However, the needle density has an upper limit and excessive needle density is not conducive to cell migration. Therefore, in the following experiments, the 1000 μm needle spacing was used to fabricate MN patches.

Effect of MDMN on cell migration

Double cells produce a synergistic effect through the cytokines interaction, further promoting migration. The effect of bi-cellular co-culture on the migratory ability of the basal cells was assessed by scratch assay. The L929 fibroblast group showed a significant improvement in cell migration in the KC MN group (42.07 % ± 11.80 %), FB MN group (54.03 % ± 2.91 %) and MDMN group (66.20 % ± 8.71 %) at day 3, compared to the control group (13.98 % ± 3.63 %) and native MN group (16.15 % ± 3.92 %) showed significantly improved cell migration, as shown in Fig. 4A. Meanwhile, MDMN was more significant in promoting cell migration than the KC MN group or the FB MN group (Fig. 4B). In addition, as shown in Fig. S4, the healing rates of the KC group (Fig. S4A) and the FB group (Fig. S4C) were as high as 76.80 % ± 2.15 % and 76.86 % ± 1.22 % in the MDMN group on day 2, and almost completely healed on day 3 (90.19 % ± 1.17 % and 90.96 % ± 1.64 %, respectively), whereas the control group had only 77.58 % ± 2.24 % and 55.94 % ± 2.40 on day 3, respectively (Fig. S4B and D). Cytokines serve as crucial regulators influencing various physiological functions and metabolic processes after injury, directly or indirectly influencing cellular growth, division, differentiation, proliferation, and migration. In the context of accelerated cell migration, our investigation initially focuses on assessing the specific cytokines released by different microneedle groups. Notably, pro-inflammatory cytokines such as TNF-α, IL-1α, and IL-1β play pivotal roles in orchestrating the inflammatory phase of wound healing. This phase involves fibroblast proliferation, synthesis and degradation of ECM proteins, fibroblast chemotaxis, and modulation of the immune response. For instance, epidermal keratinocytes exhibit constitutive production of IL-1α, with its expression rapidly escalating within four hours post-injury [51]. The rapid elevation in IL-1α concentrations correlates with a noticeable increase in basal keratinocytes, dermal fibroblasts, and a substantial influx of neutrophils to the wound site [52]. IL-1α exerts control over epidermal keratinocyte migration and proliferation, indirectly stimulates leukocyte chemotaxis, promotes fibroblast growth and collagen synthesis, and triggers fibroblasts to release KGF (keratinocyte growth factor) [53]. IL-1α and IL-1β, via signal transduction pathways, regulate angiogenesis and vascular permeability, often displaying a synergistic effect in these processes [54]. Between twelve to twenty-four hours post-injury, the primary sources of TNF-α expression include polymorphonuclear leukocytes, macrophages, and hyperproliferative epithelial cells located at the wound's periphery. TNF-α contributes to enhancing antimicrobial defense mechanisms, stimulating the expression of growth factors by fibroblasts and keratinocytes, and aiding in the regulation of migration of epidermal Langerhans cells [55–57]. Growth factors, which stimulate cell regeneration, proliferation, migration, and extracellular matrix synthesis, play a major role in wound healing. These factors include KGF, FGF, TGF-α, TGF-β, and EGF. KGF promotes the development and multiplication of epithelial cells and is found in a variety of stromal cell sources [50,58,59]. On the other hand, FGF supports angiogenesis and collagen accumulation, thereby facilitating the proliferation of fibroblasts and skin cells [60]. The TGF-β family orchestrates cellular migration, differentiation, and proliferation. Its role encompasses the attraction of inflammatory cells, facilitation of collagen production in fibroblasts, and transformation of monocytes into macrophages, all crucial for initiating inflammatory responses and tissue remodeling [61].Fibroblasts possess the capability to produce epidermal growth factor (EGF), influencing neighboring keratinocytes in a paracrine manner. This interaction enhances the migration and proliferation of keratinocytes, vital

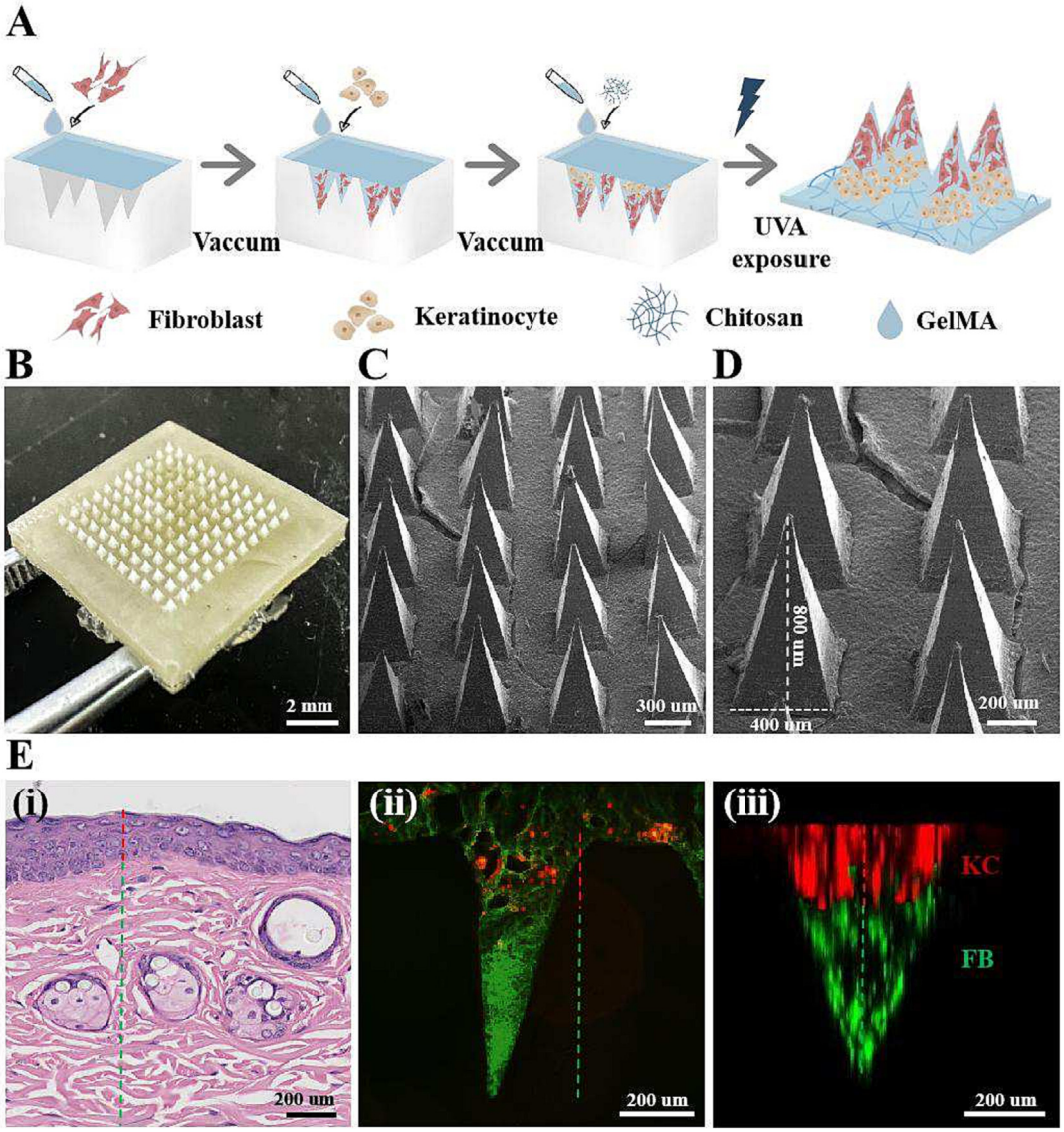

Fig. 2. Preparation and characterization of MDMN. (A) The fabrication process of MN. (B) Optical picture of MN. (C, D) SEM images of MNs. (E) (i) H&E staining of full-thickness mouse skin. (ii) Fluorescent images of MNs encapsulating KCs (red) and FBs (green) labeled with fluorescent cell membrane probes. (iii) Confocal microscopy images of MNs encapsulating KCs (red) and FBs (green) labeled with fluorescent cell membrane probes. (For interpretation of the references to colour in this figure legend, the reader is referred to the web version of this article.)

processes in the re-epithelialization phase [62–64]. Comparing the MDMN group with individual KCs and FBs, the cooperative interaction between KCs and FBs significantly upregulated the paracrine secretion of various cytokines. Notably, IL-1α (8.19 ± 0.69 vs 7.07 ± 0.73 and 7.42 ± 0.89 pg/mL), IL-1β (18.08 ± 0.58 vs15.17 ± 1.12 and 16.05 ± 0.39 ng/L), TNF-α (50.09 ± 7.02 vs 49.64 ± 4.84 and 40.23 ± 1.14 ng/ml), KGF (61.57 ± 0.95 vs 49.01 ± 2.42 and 55.17 ± 2.87 ng/ml), FGF (192.05 ± 15.46 vs 155.55 ± 13.29 and 167.92 ± 15.97 ng/L), TGF-α (347.62 ± 46.32 vs 297.55 ± 12.38 and 312.20 ± 21.12 ng/L), TGF-β (110.93 ± 10.63 vs 67.00 ± 6.91 and 82.81 ± 9.51 pg/mL), and EGF (59.69 ± 3.39 vs 44.01 ± 2.71 and 34.56 ± 2.67 pg/mL) (Fig. 4G–N). Overall, bilayer cells exhibited a superior effect in promoting migration, and this was attributed to the active factors secreted by KCs and FBs [65–68]. It was found that FBs could positively regulate KCs and further enhance their function, resulting in synergistic effects [67]. The expression of genes involved in cell migration was examine by quantitative PCR (qPCR). Among the many Rho GTPases that have been studied and are involved in migration and phagocytosis are cytokinesis control protein 42 (CDC42) and Rho (RhoA, RhoB, and RhoC). Rho binding to GTP initiates ROCK through activation of the Rho/ROCK signalling pathway, which activates F-actin polymerisation to control cell protrusion and regulates retraction and modulates microtubule dynamics by controlling actinomyosin contractility through Rho kinase (downstream of the GTPase RhoA). In addition, activation of the Rho/ROCK signaling pathway induces MLCP and MLC phosphorylation, which further regulates the level of Capzb expression and modulates cell migration capacity [69–75]. Therefore, we tested the expression levels of Rhoa, CDC42, and Capzb mRNA to verify whether MDMN can improve cell migration. As shown in Fig. 4D–F, Capzb (1.34 folds), CDC42 (1.6 folds), and Rhoa (2.68 folds) mRNA expression were increased in the MDMN group compared to the control group. These results indicate that MDMN promote wound healing by regulating genes involved in cell migration.

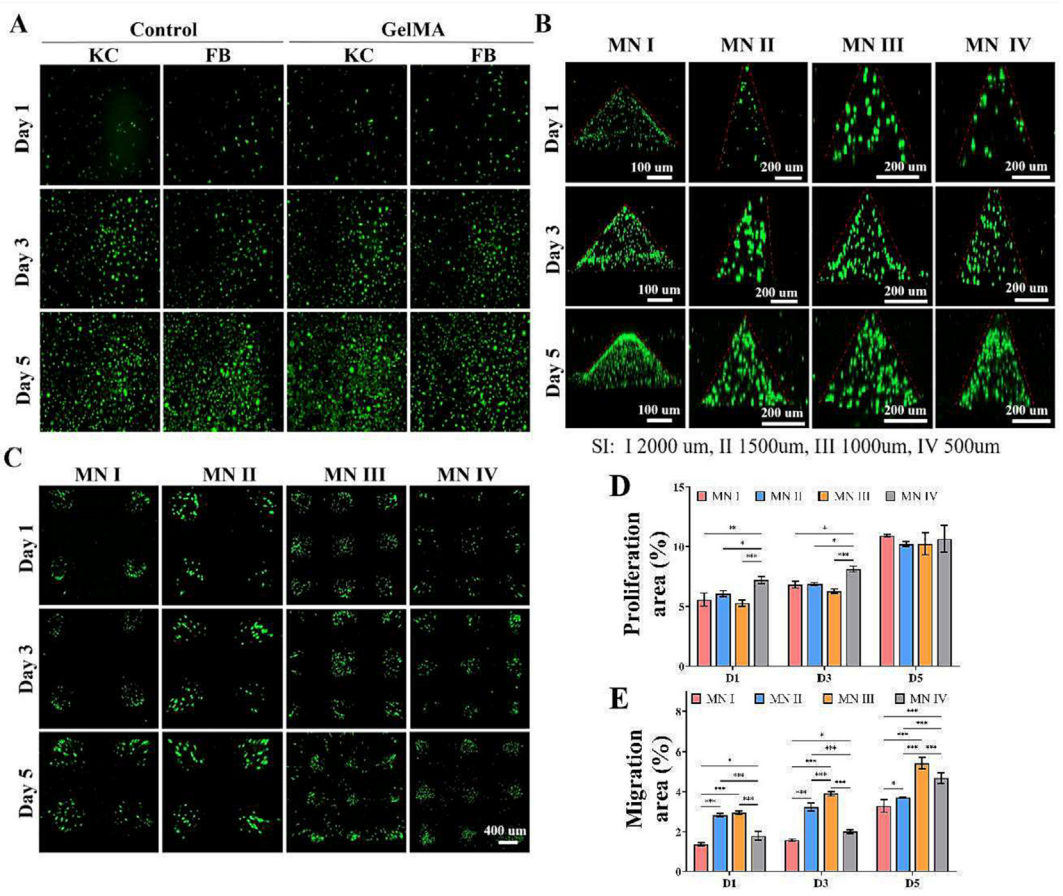

Fig. 3. MDMN biocompatibility and needle spacing. (A) Representative images of KCs and FBs cultured on plates and GelMA hydrogels on days 1, 3, and 5 (10× magnification). (B) SEM images of FBs proliferating in MN needle tips with different needle densities. (C) SEM images of directional migration of FBs in MN with different needle densities; scale bar = 400 μm. (D) Quantification of cell proliferation. (E) Quantification of cell migration. (n = 3, * $p < 0.05$, ** $p < 0.01$, *** $p < 0.001$).

The antibacterial ability of MDMN

As the wound heals, the infection can last longer and become life-threatening. These infections should not be ignored. The antimicrobial properties of the MN patch are also important in protecting the wound bed from infection. The antimicrobial activity of the MDMN patch against *Escherichia coli* and *Staphylococcus aureus* was demonstrated using the colony forming unit (CFU) method. Significantly fewer bacterial colonies were observed in the MDMN group compared to the control group (Fig. 5A). The antibacterial index was calculated according to the number of colonies, and the antibacterial index of MDMN against *E. coli* and *S. aureus* was almost 100 % (Fig. 5B and C), indicating its excellent antibacterial ability. The antimicrobial effect of MDMN is based on the presence of CS, which has positively charged functional groups that interact electrostatically with the bacterial membrane, leading to bacterial death. *E. coli* carries more negative charges and its cell membrane surface allows more cationic chitosan binding, resulting in greater sensitivity to chitosan [76]. In contrast, the absence of the teichoic acid biosynthesis pathway in *S. aureus* results in less negatively charged cell membranes and therefore less sensitivity to chitosan than *E. coli* [77]. Therefore, to achieve a similar antimicrobial effect, we decided to use a 3 % concentration of chitosan support. In conclusion, the excellent antimicrobial properties of MDMN patches demonstrate their potential to protect wounds and effectively prevent wound infection.

MDMN in vivo wound healing assessment

To further evaluate the role of MDMN in vivo, we applied it to full thickness wounds on the back of normal and diabetic mice (Fig. S5). Photographs were taken at day 0 as well as on days 7 and 14 after treatment to assess the effect of microneedling and commercial growth factors in different groups for normal wounds (Fig. S6A). At day 14, the wound areas of KC MN, FB MN, MDMN and GF were almost healed, whereas the wounds of the control group, native MN, were still unhealed (Fig. S6B). When the percentage of the wound area was quantified using Image J (Fig. S6C), the MDMN group and the GF group showed a significant improvement in minimising the wound area. Meanwhile, there was no significant difference in wound area change in the MDMN group compared to the GF group, highlighting the potential of MDMN to promote healing. H&E staining was used to observe the formation of granulation tissue and to measure the degree of tissue epithelialisation in order to assess the epithelialisation process (Fig. S6E). The results showed that the epithelial tissues were completely formed in the MDMN and GF groups after 14 days of treatment. In contrast, there was still incomplete healing in the other groups. Masson trichrome staining was used to assess collagen deposition and alignment in the tissue (Fig. S6F). The MDMN group (48.97 % ± 1.83 %) and the GF group (49.04 % ± 2.16 %) possessed optimal collagen deposition and directional alignment (Fig. S6D). In conclusion, MDMN had similar effects to commercial products in promoting wound healing, tissue regeneration, and functional integrity. Therefore, we will focus on the differences in

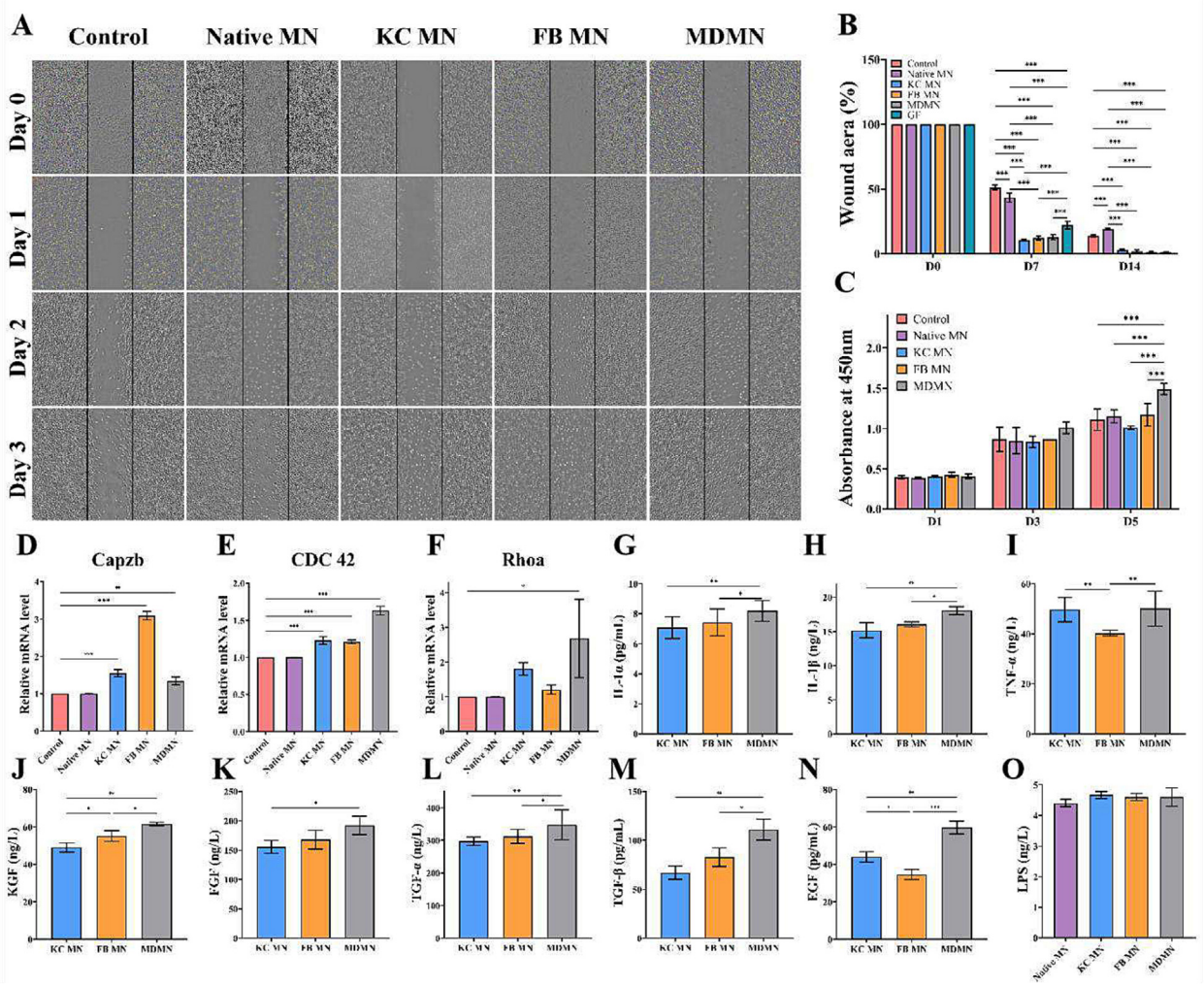

Fig. 4. Effect of MDMN on cell migration. (A) Representative optical image showing cell migration towards the wound gap; scale bar = 400 μm. (B) Percentage of the recovered area in a scratch assay. (C) CCK8 assay for cell viability on days 1, 3, and 5. (D) Semi-quantitative expression of Capzb mRNA. (E) Semi-quantitative expression of CDC42 mRNA. (F) Semi-quantitative expression of Rhoa mRNA. Levels of (G) IL-1α, (H) IL-1β, (I) TNF-α, (J) KGF, (K) FGF, (L) TGF-α, (M) TGF-β, (N) EGF, and (O) LPS in the supernatant of 24-h incubation. (n = 3, * $p < 0.05$, ** $p < 0.01$, *** $p < 0.001$).

healing promoting effects of MDMN and other microneedles in diabetic wounds.

Photographs were taken at 0, 8, and 18 days post treatment, respectively, to analyse the effect of the different groups in treating diabetic wounds (Fig. 6A). The schematic images showed that the wound area of the MDMN group was significantly smaller than that of the other groups after 18 days of treatment (Fig. 6B). On day 8, the wound area in the MDMN group (40.68 % ± 0.52 %) decreased compared to the control (45.85 % ± 0.20 %), native MN (45.04 % ± 0.55 %), KC MN (47.26 % ± 0.65 %) and FB MN groups (59.05 % ± 0.28 %). The MDMN group showed significant progress in the healing process, with only 0.96 % ± 0.58 % of the wound area remaining after 18 days. On the other hand, the control, native MN, KC MN, and FB MN groups had significantly larger unhealed areas, with 4.61 % ± 0.32 %, 7.66 % ± 0.46 %, 16.24 % ± 0.37 %, and 6.17 % ± 0.25 % respectively (Fig. 6C). These results indicated that MDMN effectively promoted wound healing. HE staining revealed that the wound healing rates of the FB MN and MDMN groups were higher than those of the control, native MN groups and KC MN groups. During wound healing, FBs are more responsive to wound-soluble mediators, mainly manifested by the granulation tissue formation and upregulation of inflammatory factors [78]. Therefore, the healing effect of the FB MN and MDMN groups was excellent. Surprisingly, the MDMN group had thicker granulation tissue and more neocapillaries as well as a flatter new epidermis compared to the FB MN group, suggesting that the MDMN group had both FB-upregulated granulation tissue formation and rapid re-epithelialisation of KCs. This promotes tissue regeneration and healing through the synergistic effects of both (Fig. 6D).

MDMN promoted angiogenesis and collagen deposition in diabetic wounds

Next we look dermal regeneration. FBs promoted collagen regeneration. However, excessive collagen proliferation often leads to disordered collagen arrangement and fibrosis, which eventually leads to scar healing. Masson staining was used to determine collagen deposition and arrangement during healing. In addition, cytokines secreted by FB can promote cell proliferation and angiogenesis. Therefore, the expression levels of proteins related to cell proliferation and angiogenesis were examined.

In the MDMN group, collagen deposition is increased and the neoepidermal structure is ordered, according to Masson staining (Fig. 7A). Compared with the control (35.81 % ± 3.79 %), native MN (36.78 % ± 2.81 %), KC MN (38.81 % ± 3.68 %), and FB MN groups (40.94 % ± 5.59 %), the collagen deposition was significantly

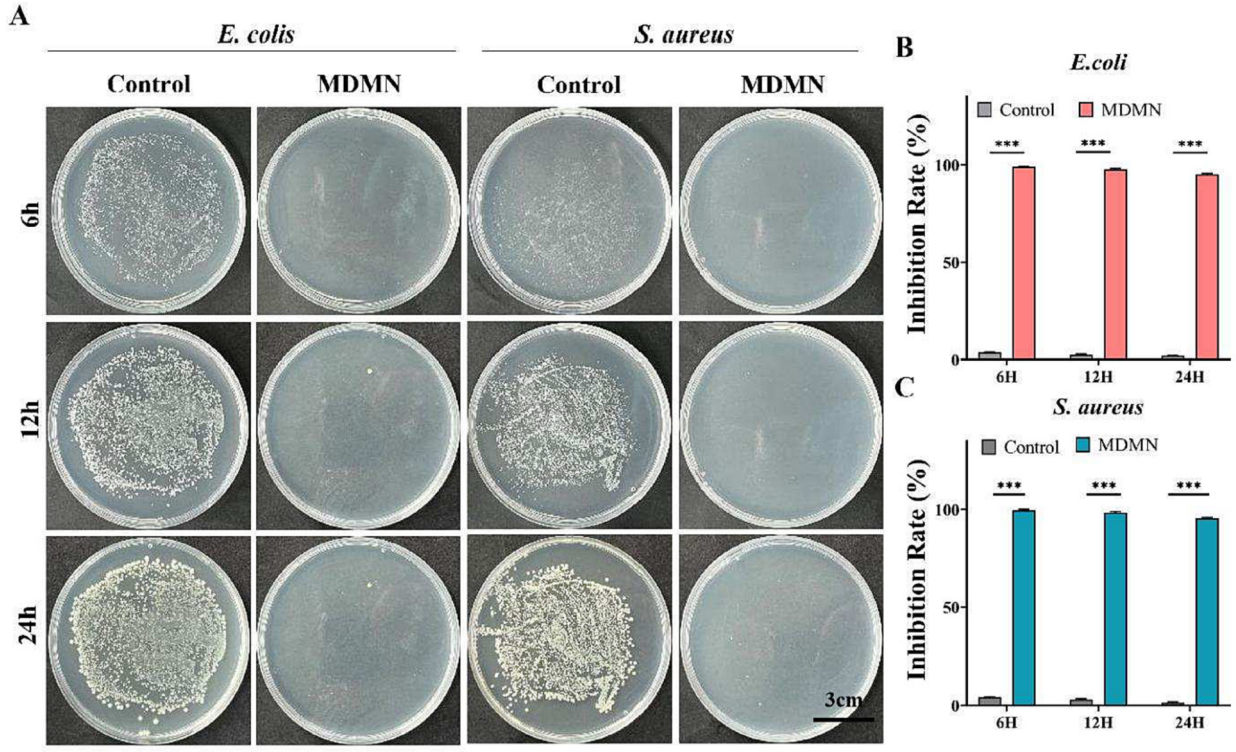

Fig. 5. Evaluation of the antimicrobial potential of MDMN patches. (A) Colony counts at 6 h, 12 h, and 24 h after treatment; scale bar = 3 cm. (B) Statistical analysis of the inhibition rate of Escherichia coli between the control group and the MDMN group. (C) Statistical analysis of the inhibition rate of Staphylococcus aureus between the control group and the MDMN group. (n = 3, *** $p < 0.001$).

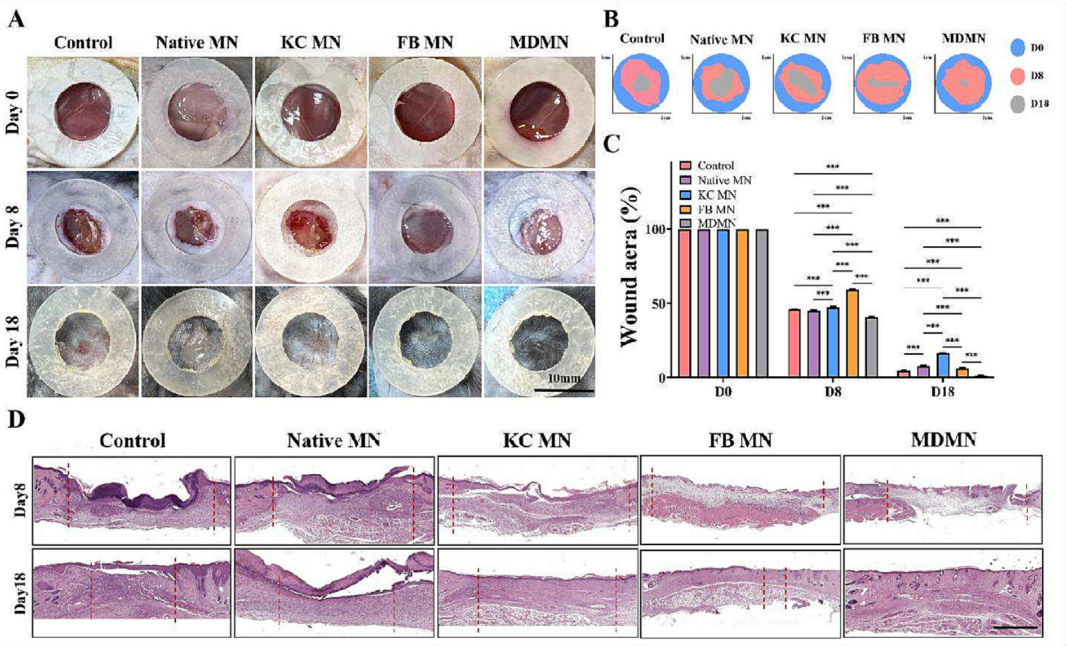

Fig. 6. Efficacy of MDMN in promoting full-thickness wound healing. (A) Representative images of skin regeneration. Postoperative treatments were assigned to mouse wounds in the following groups: control, KC MN, FB MN, and MDMN. Representative images of the wound area were captured on days 0, 8, and 18, and mice were sacrificed for section staining after the pictures were taken on days 8 and 18. The annular silicone patch used had an inner diameter of 10 mm. (B) Pattern diagram of skin regeneration. (C) Quantification of wound closure area, *** $p < 0.001$. (D) HE staining of each group on days 8 and 18. Scale bar = 500 μm.

enhanced in the MDMN group (48.25 % ± 3.945 %) (Fig. 7C). In addition to collagen deposition, cell proliferation and angiogenesis are important indicators of tissue layer remodelling. We then examined the levels of proteins associated with cell proliferation and angiogenesis using immunofluorescence staining. In the MDMN group, PCNA + cells were widely distributed in the nascent tissue, indicating that a large number of cells had proliferated in the nascent tissue, and CD31 staining indicated the formation of new

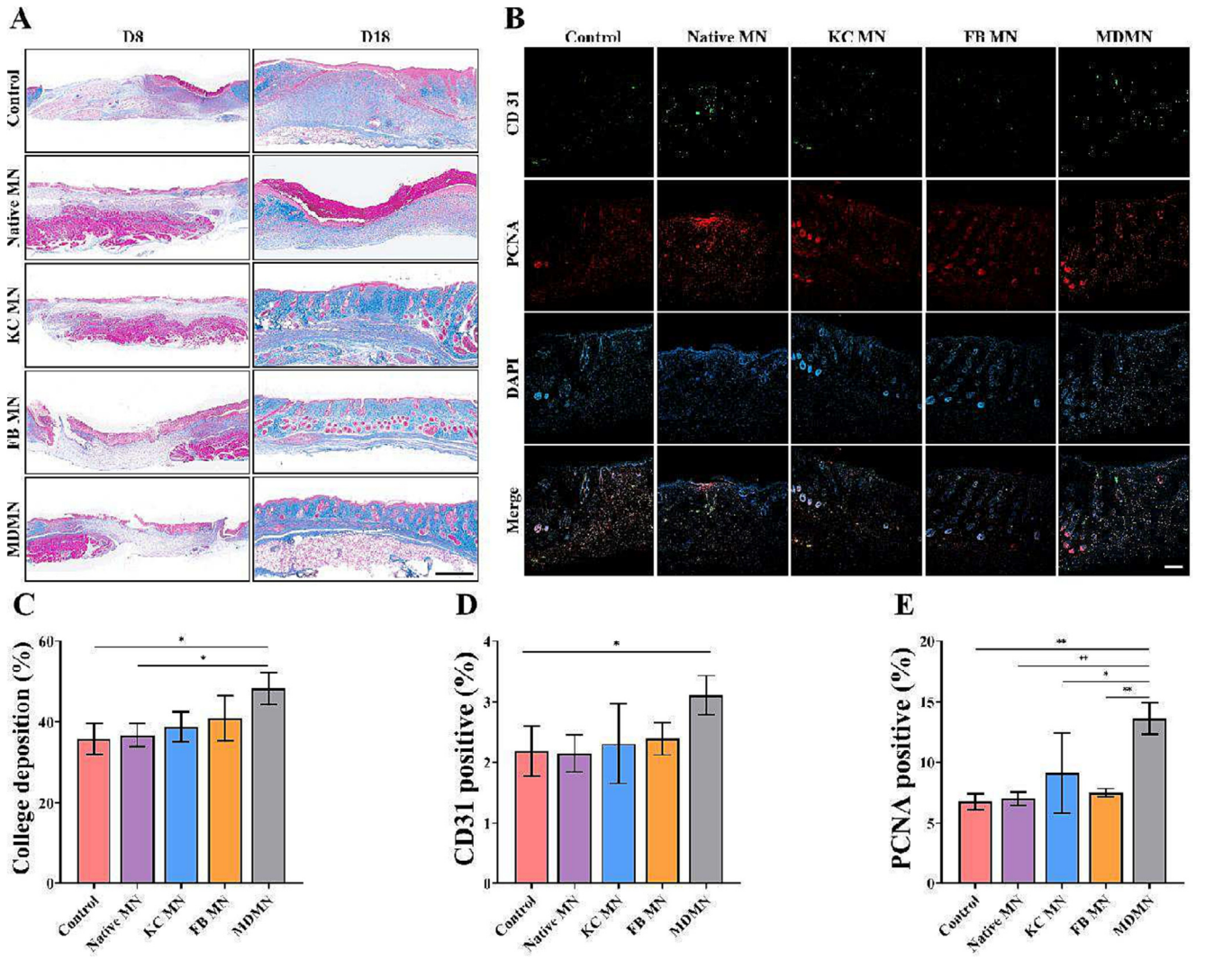

Fig. 7. Wound healing assessment in MDMN. (A) Masson staining on days 8 and 18 of each group; scale bar = 500 μm. (B) Representative fluorescent staining of CD31, PCNA, and DAPI at the wound edge of each group; scale bar = 200 μm. (C) Collagen deposition was quantified in each group. (D) Quantitative analysis of CD31 protein expression in each group. (E) Quantitative analysis of PCNA protein expression in each group. (* $p < 0.05$, ** $p < 0.01$).

microvessels (Fig. 7B). Quantitative analysis showed that the relative expression levels of PCNA+ (13.63 % ± 1.31 %) and CD31 (3.1 1 % ± 0.32 %) were significantly upregulated in the MDMN group compared with the control group, PCNA+ (6.77 % ± 0.67 %) and CD31 (2.19 % ± 0.41 %) (Fig. 7D and E). These results suggest that the multi-centre healing mode of MDMN promotes cell proliferation and migration through the synergistic action of longitudinal double layer cells.

MDMN's biological actions in fostering healing

Keratinocytes, located in the epidermis, undergo continual proliferation, replacing mature cells and renewing tissue while forming a protective barrier [79]. The process of lifelong self-renewal is essential for maintaining the normal structure of tissues and ensuring stability within the intracellular environment [80]. Therefore, understanding the mechanisms responsible for the proliferation and migration of keratinocytes is crucial for promoting the comprehensive repair of both functional and structural skin wounds [81,82]. Following an injury, fibroblasts undergo rapid proliferation, producing significant amounts of collagen fibers and matrix constituents, thereby filling the wound bed with newly formed granulation tissue and capillaries. In the later stages of the injury, fibroblasts release a substantial quantity of collagenase, which plays a crucial role in tissue repair and remodeling [83–85]. In the early stages of wound formation, an inflammatory zone, primarily comprising neutrophilic cells, emerges at the boundary between healthy and necrotic tissue located at the wound base. This area acts as a protective barrier against external microorganisms and produces enzymes that degrade the necrotic tissue, segregating it from the surrounding tissue and aiding its removal. Neutrophils secrete various substances that not only recruit macrophages to the wound area to engage in the inflammatory reaction but also facilitate the shift from M1 to M2 macrophage subtypes, initiating the repair and proliferation process [86]. M1 macrophages are inflammatory cells with cytotoxic and pro-inflammatory traits, heightening local inflammatory reactions. Conversely, M2 macrophages, referred to as pro-repair macrophages, possess anti-inflammatory and pro-proliferative qualities [87]. Activation of M2-type macrophages enhances the wound's secretion of pro-angiogenic factors like VEGF, thereby facilitating the wound healing process and promoting the regeneration of blood vessels within the wound site [88]. Vascular endothelial cells actively participate in angiogenesis by engaging in processes like proliferation, migration,

and budding, thereby contributing significantly to wound healing. Angiogenesis, the formation of blood vessels, is a crucial component of granulation tissue formation. These newly formed blood vessels play a pivotal role in supplying the wound site with oxygen, essential nutrients, and bioactive substances, all of which are instrumental in driving and supporting the wound healing process [89]. Meanwhile, endothelial cells play a critical role in guiding the migration of inflammatory cells from blood vessels to the site of damaged skin tissues through a process known as chemotaxis. Upon arrival at the damaged area, these inflammatory cells release inflammatory factors and extracellular matrix components, fostering the proliferation of basal cells [90,91].

All things considered, cytokines play a major role in controlling a number of physiological processes and metabolic activities following injury. The current study highlighted numerous cytokines and growth factors that initiate the wound-healing cascade, emphasizing their interactions with cells that exhibit migratory, hyperproliferative, inflammatory, neovascularizing, and tissue regenerative properties. The multicentre regenerative microneedle (MDMN) exhibited notably higher levels of factor release compared to single-cell microneedles (KC MN and FB MN). This observation aligns with increased healing-related cell migration and proliferation, underscoring the efficacy of bilayer cells over monolayer cells in stimulating these functions. The study affirms the therapeutic potential of MDMN through intercellular synergy, promoting the secretion of various growth factors and fostering M2 macrophage polarization, which may enhance the healing process of non-cancerous wounds.

Conclusion

In this study, we propose a novel multi-centric regeneration model that can simultaneously regenerate and fuse to form a complete full-thickness skin and significantly reduce wound healing time compared to the traditional centripetal healing mode. The bilayer design, which mimics the hierarchical structure of the skin, provides robust support for cell growth, movement and combined action of different cells. This study validates the therapeutic effectiveness of a multicenter regenerative microneedle model involving FB and KC cells. The introduced MDMN stimulates the secretion of various growth factors such as TGF-α, TGF-β, and FGF, which exhibit synergistic effects between cells. These growth factors, acting in a paracrine manner, hold promise in modulating macrophages within the wound area, facilitating a shift toward the M2 phenotype and ultimately improving wound healing. In vitro testing validated that by adjusting of the density of regeneration centres, MDMN was able to achieve the ideal distribution distance for cell migration. Bilayer microneedles synergistically utilise epidermal and dermal cells to fully regenerate functional skin. The therapeutic effecacy of MDMN was measured by full-thickness skin removal in a diabetic mouse model. MDMN improved the rate of wound closure, re-epithelialisation, and collagen alignment, and increased cell proliferation and angiogenesis, resulting in the formation of functional skin.

This innovative regenerative technique has demonstrated efficacy and a wide range of potential applications. However, the microneedle model employed in this study didn't encompass other crucial cell types essential in tissue restoration. Therefore, our future research will explore the interactions of this model with other cell types and its potential applicability across the spectrum of wound healing responses.

Funding sources

This work was supported by the fund program of National Natural Science Foundation of China (Grant No: 81772101,82072196, 82002066) and the Science Fund for Distinguished Young Scholars of Southern Medical University (Grant number: 2020J009).

CRediT authorship contribution statement

Xiaoqi Huang: Conceptualization, Writing – original draft. **Xingtang Niu:** Methodology, Formal analysis. **Yuan Ma:** Methodology. **Xinhui Wang:** Software. **Ting Su:** Supervision, Data curation. **Yu He:** Validation, Supervision. **Feng Lu:** Supervision, Validation. **Jianhua Gao:** Supervision, Resources, Validation. **Qiang Chang:** Writing – review & editing.

Declaration of Competing Interest

The authors declare that they have no known competing financial interests or personal relationships that could have appeared to influence the work reported in this paper.

Acknowledgment

The study was supported by the National Natural Science Foundation of China (Grant No: 81772101, 82072196, 82002066). We are also very grateful for the support of the Science Fund for Distinguished Young Scholars of Southern Medical University (Grant number: 2020J009).

Appendix A. Supplementary data

Supplementary data to this article can be found online at https://doi.org/10.1016/j.jare.2024.01.002.

References

[1] Chengwei W, Yihao L, Xiaoxiao Y, Wentao L, Xianhao Z, Ya R, et al. In-situ forming hydrogel incorporated with reactive oxygen species responsive and antibacterial properties for diabetic infected chronic wound healing. Chem Eng J 2022;450:138077.
[2] Sun H, Yang Y, Wu Y, Fu Z, Zhang Y, Liu Y, et al. Zinc alginate hydrogels with embedded RL-QN15 peptide-loaded hollow polydopamine nanoparticles for diabetic wound healing therapy. Mater Des 2022;222:111085.
[3] Li Z, Fan X, Luo Z, Loh XJ, Ma Y, Ye E, et al. Nanoenzyme–chitosan hydrogel complex with cascade catalytic and self-reinforced antibacterial performance for accelerated healing of diabetic wounds. Nanoscale 2022;14:14970–83.
[4] Ou X, Guan L, Guo W, Zhang X, Wu S, Guo D, et al. Graphene oxide-based injectable conductive hydrogel dressing with immunomodulatory for chronic infected diabetic wounds. Mater Des 2022;224:111284.
[5] Zhou W, Duan Z, Zhao J, Fu R, Zhu C, Fan D. Glucose and MMP-9 dual-responsive hydrogel with temperature sensitive self-adaptive shape and controlled drug release accelerates diabetic wound healing. Bioact Mater 2022;17:1–17.
[6] Luo H, Bian H, Sun C, Zheng S, Xiong B, Huang Z, et al. Usage of intermingled skin allografts and autografts in a senior patient with major burn injury. Open Med 2021;16:1745–8.
[7] Fu C, Qi Z, Zhao C, Kong W, Li H, Guo W, et al. Enhanced wound repair ability of arginine-chitosan nanocomposite membrane through the antimicrobial peptides-loaded polydopamine-modified graphene oxide. J Biol Eng 2021;15:17.
[8] Zhou X, Wang Z, Chan YK, Yang Y, Jiao Z, Li L, et al. Infection micromilieu-activated nanocatalytic membrane for orchestrating rapid sterilization and stalled chronic wound regeneration. Adv Funct Mater 2022;32:2109469.
[9] Panayi AC, Wu M, Liu Q, Yu Z, Karvar M, Aoki S, et al. Negative pressure wound therapy promotes murine diabetic wound healing by enhancing lymphangiogenesis. J Am Coll Surg 2021;233:S209.
[10] Zimoch J, Zielinska D, Michalak-Micka K, Rütsche D, Böni R, Biedermann T, et al. Bio-engineering a prevascularized human tri-layered skin substitute containing a hypodermis. Acta Biomater 2021;134:215–27.
[11] Fernández-González A, Lizana-Moreno A, Fernández N, Guerrero-Calvo J, Ruiz-Garcia A, Espinosa O, et al. Clinical, histological and homeostasis evaluation of an autologous tissue bio-engineered skin substitute in a patient with 70% of total body surface area (TBSA) burn. Cytotherapy 2017;19:S233.
[12] Gao X, Zhang M, Lin Y, Li D, Zhang L. Combined complex skin repair in patient with extensive burns: a case report. J Burn Care Res 2021;42:1053–6.
[13] Tom LK, Maine RG, Wang CS, Parent BA, Bulger EM, Keys KA. Comparison of traditional and skin-sparing approaches for surgical treatment of necrotizing soft-tissue infections. Surg Infect (Larchmt) 2020;21:363–9.

[14] Sheikholeslam M, Wright MEE, Jeschke MG, Amini-Nik S. Biomaterials for skin substitutes. Adv Healthc Mater 2018;7:1700897.
[15] Rettinger CL, Fletcher JL, Carlsson AH, Chan RK. Accelerated epithelialization and improved wound healing metrics in porcine full-thickness wounds transplanted with full-thickness skin micrografts. Wound Repair Regener 2017;25:816–27.
[16] Kruse CR, Sakthivel D, Sinha I, Helm D, Sørensen JA, Eriksson E, et al. Evaluation of the efficacy of cell and micrograft transplantation for full-thickness wound healing. J Surg Res 2018;227:35–43.
[17] Noureldin MA, Said TA, Makeen K, Kadry HM. Comparative study between skin micrografting (Meek technique) and meshed skin grafts in paediatric burns. Burns 2022;48:1632–44.
[18] Fulchignoni C, Rocchi L, Cauteruccio M, Merendi G. Matriderm dermal substitute in the treatment of post traumatic hand's fingertip tissue loss. J Cosmet Dermatol 2022;21:750–7.
[19] Riccio M, Marchesini A, Zingaretti N, Carella S, Senesi L, Onesti MG, et al. A multicentre study: the use of micrografts in the reconstruction of full-thickness posttraumatic skin defects of the limbs—a whole innovative concept in regenerative surgery. Stem Cells Int 2019;2019:1–10.
[20] Chang P, Li S, Sun Q, Guo K, Wang H, Li S, et al. Large full-thickness wounded skin regeneration using 3D-printed elastic scaffold with minimal functional unit of skin. J Tissue Eng 2022;13:204173142110630. https://doi.org/10/gqp9qw.
[21] Komorowska-Timek E, Gabriel A, Bennett DC, Miles D, Garberoglio C, Cheng C, et al. Artificial dermis as an alternative for coverage of complex scalp defects following excision of malignant tumors: plastic and reconstructive surgery 2005;115:1010–7. https://doi.org/10/b7ppq3.
[22] Sallehuddin N, Md Fadilah NI, Hwei NM, Wen APY, Yusop SM, Rajab NF, et al. Characterization and cytocompatibility of collagen–gelatin–elastin (CollaGee) acellular skin substitute towards human dermal fibroblasts. In Vitro Assessment Biomedicines 2022;10:1327.
[23] Sharifi E, Sadati SA, Yousefiasl S, Sartorius R, Zafari M, Rezakhani L, et al. Cell loaded hydrogel containing Ag-doped bioactive glass–ceramic nanoparticles as skin substitute: antibacterial properties, immune response, and scarless cutaneous wound regeneration. Bioeng Transl Med 2022;7:e10386.
[24] Chen J, He J, Yang Y, Qiao L, Hu J, Zhang J, et al. Antibacterial adhesive self-healing hydrogels to promote diabetic wound healing. Acta Biomater 2022;146:119–30.
[25] Han X, Ju LS, Irudayaraj J. Oxygenated wound dressings for hypoxia mitigation and enhanced wound healing. Mol Pharm 2023;20:3338–55.
[26] Pastar I, Stojadinovic O, Yin NC, Ramirez H, Nusbaum AG, Sawaya A, et al. Epithelialization in wound healing: a comprehensive review. Adv Wound Care 2014;3:445–64.
[27] Ma W, Zhang X, Liu Y, Fan L, Gan J, Liu W, et al. Polydopamine decorated microneedles with Fe-MSC-derived nanovesicles encapsulation for wound healing. Adv Sci 2022;9:2103317.
[28] Sheng T, Luo B, Zhang W, Ge X, Yu J, Zhang Y, et al. Microneedle-mediated vaccination: innovation and translation. Adv Drug Deliv Rev 2021;179:113919.
[29] Zhang X, Chen G, Bian F, Cai L, Zhao Y. Encoded microneedle arrays for detection of skin interstitial fluid biomarkers. Adv Mater 2019;31:1902825.
[30] Williams CG, Malik AN, Kim TK, Manson PN, Elisseeff JH. Variable cytocompatibility of six cell lines with photoinitiators used for polymerizing hydrogels and cell encapsulation. Biomaterials 2005;26:1211–8.
[31] Nazir F, Ashraf I, Iqbal M, Ahmad T, Anjum S. 6-deoxy-aminocellulose derivatives embedded soft gelatin methacryloyl (GelMA) hydrogels for improved wound healing applications: In vitro and in vivo studies. Int J Biol Macromol 2021;185:419–33.
[32] Wang J-H, Tsai C-W, Tsai N-Y, Chiang C-Y, Lin R-S, Pereira RF, et al. An injectable, dual crosslinkable hybrid pectin methacrylate (PECMA)/gelatin methacryloyl (GelMA) hydrogel for skin hemostasis applications. Int J Biol Macromol 2021;185:441–50.
[33] Fan Y, Yue Z, Lucarelli E, Wallace GG. Hybrid printing using cellulose nanocrystals reinforced GelMA/HAMA hydrogels for improved structural integration. Adv Healthc Mater 2020;9:2001410.
[34] Yuan Z, Yuan X, Zhao Y, Cai Q, Wang Y, Luo R, et al. Injectable GelMA cryogel microspheres for modularized cell delivery and potential vascularized bone regeneration. Small 2021;17:2006596.
[35] Xu W, Molino BZ, Cheng F, Molino PJ, Yue Z, Su D, et al. On low-concentration inks formulated by nanocellulose assisted with gelatin methacrylate (GelMA) for 3D printing toward wound healing application. ACS Appl Mater Interfaces 2019;11:8838–48.
[36] Yi S, Liu Q, Luo Z, He JJ, Ma H, Li W, et al. Micropore-forming gelatin methacryloyl (GelMA) bioink toolbox 2.0: designable tunability and adaptability for 3D bioprinting applications. Small 2022;18:2106357.
[37] Kurian AG, Singh RK, Patel KD, Lee J-H, Kim H-W. Multifunctional GelMA platforms with nanomaterials for advanced tissue therapeutics. Bioact Mater 2022;8:267–95.
[38] Stefanov I, Hinojosa-Caballero D, Maspoch S, Hoyo J, Tzanov T. Enzymatic synthesis of a thiolated chitosan-based wound dressing crosslinked with chicoric acid. J Mater Chem B 2018;6:7943–53.
[39] Wei H, Liu S, Tong Z, Chen T, Yang M, Guo Y, et al. Hydrogel-based microneedles of chitosan derivatives for drug delivery. React Funct Polym 2022;172:105200.
[40] Chi J, Zhang X, Chen C, Shao C, Zhao Y, Wang Y. Antibacterial and angiogenic chitosan microneedle array patch for promoting wound healing. Bioact Mater 2020;5:253–9.
[41] Zhang J, Ma S, Liu Z, Geng H, Lu X, Zhang X, et al. Guided bone regeneration with asymmetric collagen-chitosan membranes containing aspirin-loaded chitosan nanoparticles. Int J Nanomed 2017;12:8855–66.
[42] Sandri G, Rossi S, Bonferoni MC, Miele D, Faccendini A, Del Favero E, et al. Chitosan/glycosaminoglycan scaffolds for skin reparation. Carbohydr Polym 2019;220:219–27.
[43] Xu Y, Wu X, Zhang X, Zu Y, Tan Q, Zhao Y. Living microneedle patch with adipose-derived stem cells embedding for diabetic ulcer healing. Adv Funct Mater 2023;33:2209986.
[44] Wang M, Song L, Strange C, Dong X, Wang H. Therapeutic effects of adipose stem cells from diabetic mice for the treatment of type 2 diabetes. Mol Ther 2018;26:1921–30.
[45] Zhao Y, Huang L, Lin G, Tong M, Xie Y, Pan H, et al. Skin-adaptive film dressing with smart-release of growth factors accelerated diabetic wound healing. Int J Biol Macromol 2022;222:2729–43.
[46] Zeng Y, Wang C, Lei K, Xiao C, Jiang X, Zhang W, et al. Multifunctional MOF-based microneedle patch with synergistic chemo-photodynamic antibacterial effect and sustained release of growth factor for chronic wound healing. Adv Healthc Mater 2023;12:2300250.
[47] Sen S, Basak P, Prasad Sinha B, Maurye P, Kumar Jaiswal K, Das P, et al. Anti-inflammatory effect of epidermal growth factor conjugated silk fibroin immobilized polyurethane ameliorates diabetic burn wound healing. Int J Biol Macromol 2020;143:1009–32.
[48] Devalliere J, Dooley K, Hu Y, Kelangi SS, Uygun BE, Yarmush ML. Co-delivery of a growth factor and a tissue-protective molecule using elastin biopolymers accelerates wound healing in diabetic mice. Biomaterials 2017;141:149–60.
[49] Wang Y, Song B, Chen J, Cao J, Li X, Sun C. Polymethoxyflavones in citrus regulate lipopolysaccharide-induced oscillating decay of circadian rhythm genes by inhibiting Nlrp3 expression. Oxid Med Cell Longev 2021;2021:1–15.
[50] Zhang Q, Shi L, He H, Liu X, Huang Y, Xu D, et al. Down-regulating scar formation by microneedles directly via a mechanical communication pathway. ACS Nano 2022;16:10163–78.
[51] Sauder DN, Kilian PL, McLane JA, Quick TW, Jakubovic H, Davis SC, et al. Interleukin-1 enhances epidermal wound healing. Lymphokine Res 1990;9:465–73.
[52] Robertson FM, Pellegrini AE, Ross MS, Oberyszyn AS, Boros LG, Bijur GN, et al. Interleukin-1α gene expression during wound healing. Wound Repair Regen 1995;3:473–84.
[53] Zeng Q, Chen W. The functional behavior of a macrophage/fibroblast co-culture model derived from normal and diabetic mice with a marine gelatin–oxidized alginate hydrogel. Biomaterials 2010;31:5772–81.
[54] Hu P, Chiarini A, Wu J, Freddi G, Nie K, Armato U, et al. Exosomes of adult human fibroblasts cultured on 3D silk fibroin nonwovens intensely stimulate neoangiogenesis. Burns Trauma 2021;9:. doi: https://doi.org/10.1093/burnst/tkab003tkab003.
[55] Kerenidis I, Landman J. Quantum spectral clustering. Phys Rev A 2021;103:042415.
[56] Cumberbatch M. Differential regulation of epidermal langerhans cell migration by interleukins (IL)-1α and IL-1β during Irritant- and allergen-induced cutaneous immune responses. Toxicol Appl Pharmacol 2002;182:126–35.
[57] Yin H, Chen C-Y, Liu Y-W, Tan Y-J, Deng Z-L, Yang F, et al. Synechococcus elongatus PCC7942 secretes extracellular vesicles to accelerate cutaneous wound healing by promoting angiogenesis. Theranostics 2019;9:2678–93.
[58] Mercado AM, Padgett DA, Sheridan JF, Marucha PT. Altered kinetics of IL-1α, IL-1β, and KGF-1 gene expression in early wounds of restrained mice. Brain Behav Immun 2002;16:150–62.
[59] Lu Y, Yang Y, Xiao L, Li S, Liao X, Liu H. Autocrine and paracrine effects of vascular endothelial cells promote cutaneous wound healing. Biomed Res Int 2021;2021:1–10.
[60] Chen G, An N, Ye W, Huang S, Chen Y, Hu Z, et al. bFGF alleviates diabetes-associated endothelial impairment by downregulating inflammation via S-nitrosylation pathway. Redox Biol 2021;41:101904.
[61] Akhoondian M, Zabihi MR, Yavari S, Karampoor M, Fouladpour A, Fallahpour M, et al. Identification of TGF-β1 expression pathway in the improvement of burn wound healing. Burns 2022;48:2007–10.
[62] Barrientos S, Stojadinovic O, Golinko MS, Brem H, Tomic-Canic M. PERSPECTIVE ARTICLE: growth factors and cytokines in wound healing. Wound Repair Regener 2008;16:585–601.
[63] Bunker EN, Wheeler GE, Chapnick DA, Liu X. Suppression of α-catenin and adherens junctions enhances epithelial cell proliferation and motility via TACE-mediated TGF-α autocrine/paracrine signaling. Mol Biol Cell 2021;32:348–61.
[64] Auf Dem Keller U, Krampert M, Kümin A, Braun S, Werner S. Keratinocyte growth factor: effects on keratinocytes and mechanisms of action. Eur J Cell Biol 2004;83:607–12.

[65] Ong HT, Dilley RJ. Novel non-angiogenic role for mesenchymal stem cell-derived vascular endothelial growth factor on keratinocytes during wound healing. Cytokine Growth Factor Rev 2018;44:69–79.
[66] Nakajo T, Katayoshi T, Kitajima N, Tsuji-Naito K. 1,25-Dihydroxyvitamin D3 attenuates IL-1β secretion by suppressing NLRP1 inflammasome activation by upregulating the NRF2-HO-1 pathway in epidermal keratinocytes. Redox Biol 2021;48:102203.
[67] Witte RP, Kao WJ. Keratinocyte-fibroblast paracrine interaction: the effects of substrate and culture condition. Biomaterials 2005;26:3673–82.
[68] Li X, Wang C, Xiao J, McKeehan WL, Wang F. Fibroblast growth factors, old kids on the new block. Semin Cell Dev Biol 2016;53:155–67.
[69] Wilkinson S, Paterson HF, Marshall CJ. Cdc42–MRCK and Rho–ROCK signalling cooperate in myosin phosphorylation and cell invasion. Nat Cell Biol 2005;7:255–61.
[70] Wan Mohamad Noor WNI, Nguyen NTH, Cheong TH, Chek MF, Hakoshima T, Inaba T, et al. Small GTPase Cdc42, WASP, and scaffold proteins for higher-order assembly of the F-BAR domain protein. Sci Adv 2023;9:eadf5143.
[71] Hladyshau S, Stoop JP, Kamada K, Nie S, Tsygankov DV. Spatiotemporal coordination of Rac1 and Cdc42 at the whole cell level during cell ruffling. Cell Biology 2023. doi: https://doi.org/10.1101/2023.03.31.535147.
[72] Cui H, Liu Y, Zheng Y, Li H, Zhang M, Wang X, et al. Intelectin enhances the phagocytosis of macrophages via CDC42-WASF2-ARPC2 signaling axis in Megalobrama amblycephala. Int J Biol Macromol 2023;236:124027.
[73] Acharya BR, Nestor-Bergmann A, Liang X, Gupta S, Duszyc K, Gauquelin E, et al. A mechanosensitive RhoA pathway that protects epithelia against acute tensile stress. Dev Cell 2018;47. 439–452.e6.
[74] Rothenberg KE, Chen Y, McDonald JA, Fernandez-Gonzalez R. Rap1 coordinates cell-cell adhesion and cytoskeletal reorganization to drive collective cell migration in vivo. Curr Biol 2023;33. 2587–2601.e5.
[75] Pasquina-Lemonche L, Burns J, Turner RD, Kumar S, Tank R, Mullin N, et al. The architecture of the Gram-positive bacterial cell wall. Nature 2020;582:294–7.
[76] Ke C-L, Deng F-S, Chuang C-Y, Lin C-H. Antimicrobial actions and applications of chitosan. Polymers 2021;13:904.
[77] Van Den Broek LJ, Kroeze KL, Waaijman T, Breetveld M, Sampat-Sardjoepersad SC, Niessen FB, et al. Differential response of human adipose tissue-derived mesenchymal stem cells, dermal fibroblasts, and keratinocytes to burn wound exudates: potential role of skin-specific chemokine CCL27. Tissue Eng A 2014;20:197–209.
[78] Iwata Y, Akamatsu H, Hasebe Y, Hasegawa S, Sugiura K. Skin-resident stem cells and wound healing. Japanese J Clin Immunol 2017;40:1–11.
[79] Yamada T, Hasegawa S, Miyachi K, Date Y, Inoue Y, Yagami A, et al. Laminin-332 regulates differentiation of human interfollicular epidermal stem cells. Mech Ageing Dev 2018;171:37–46.
[80] Yin C, Zhang T, Qiao L, Du J, Li S, Zhao H, et al. TLR7-expressing cells comprise an interfollicular epidermal stem cell population in murine epidermis. Sci Rep 2014;4:5831.
[81] Liu Y, Wang H, Wang J. Exosomes as a novel pathway for regulating development and diseases of the skin (Review). Biomed Rep 2018.
[82] Motamed S, Taghiabadi E, Molaei H, Sodeifi N, Hassanpour SE, Shafieyan S, et al. Cell-based skin substitutes accelerate regeneration of extensive burn wounds in rats. Am J Surg 2017;214:762–9.
[83] Stunova A, Vistejnova L. Dermal fibroblasts—a heterogeneous population with regulatory function in wound healing. Cytokine Growth Factor Rev 2018;39:137–50. doi: https://doi.org/10.1016/j.cytogfr.2018.01.003.
[84] Shin D, Lee S, Huang Y-H, Lim H-W, Lee Y, Jang K, et al. Protective properties of geniposide against UV-B-induced photooxidative stress in human dermal fibroblasts. Pharm Biol 2018;56:176–82.
[85] Miao M, Yuan B, Mani R, Lu S. Macrophage activation dysfunction in impaired wound healing: a potential therapeutic target. Int J Low Extrem Wounds 2013;12:239–41.
[86] Ma J, Chen T, Mandelin J, Ceponis A, Miller NE, Hukkanen M, et al. Regulation of macrophage activation. Cell Mol Life Sci 2003;60:2334–46.
[87] Kim H, Wang SY, Kwak G, Yang Y, Kwon IC, Kim SH. Exosome-guided phenotypic switch of M1 to M2 macrophages for cutaneous wound healing. Adv Sci 2019;6:1900513.
[88] Belvedere R, Pessolano E, Porta A, Tosco A, Parente L, Petrella F, et al. Mesoglycan induces the secretion of microvesicles by keratinocytes able to activate human fibroblasts and endothelial cells: a novel mechanism in skin wound healing. Eur J Pharmacol 2020;869:172894.
[89] Chang M, Guo F, Zhou Z, Huang X, Yi L, Dou Y, et al. HBP induces the expression of monocyte chemoattractant protein-1 via the FAK/PI3K/AKT and p38 MAPK/NF-κB pathways in vascular endothelial cells. Cell Signal 2018;43:85–94.
[90] Mancini SJ, Boyd D, Katwan OJ, Strembitska A, Almabrouk TA, Kennedy S, et al. Canagliflozin inhibits interleukin-1β-stimulated cytokine and chemokine secretion in vascular endothelial cells by AMP-activated protein kinase-dependent and -independent mechanisms. Sci Rep 2018;8:5276.
[91] Veronesi F, Borsari V, Sartori M, Orciani M, Mattioli-Belmonte M, Fini M. The use of cell conditioned medium for musculoskeletal tissue regeneration. J Cell Physiol 2018;233:4423–42.